Journal of Quantitative Spectroscopy & Radiative Transfer 345 (2025) 109576

Contents lists available at ScienceDirect

Journal of Quantitative Spectroscopy and Radiative Transfer

journal homepage: www.elsevier.com/locate/jqsrt

Measurements and calculations of H_2O broadened by CO_2 collisional parameters for planetary atmospheres

É. Ducreux [a,b,c], B. Vispoel [c], B. Grouiez [a], R.R. Gamache [d], M. Lepère [c], S. Robert [b], L. Régalia [a,*]

[a] Université de Reims Champagne-Ardenne, CNRS, GSMA, Reims, France
[b] Planetary Atmospheres, Royal Belgian Institute for Space Aeronomy, 3 Avenue Circulaire, 1180 Brussels, Belgium
[c] Institute of Life, Earth and Environment (ILEE), University of Namur (UNamur), 61 rue de Bruxelles, Namur 5000, Belgium
[d] Department of Environmental, Earth, and Atmospheric Sciences, University of Massachusetts Lowell, 1 University Avenue, Lowell, MA 01854, USA

ARTICLE INFO

Keywords:
High resolution infrared spectroscopy
Complex Robert-Bonamy-Ma calculations
Line shape parameters
Water vapor
Carbon dioxide
Planetary atmospheres

ABSTRACT

Collisional parameters of H_2O with CO_2 are currently missing from international spectroscopic databases, although they are essential for accurate modeling of water vapor in CO_2-rich planetary atmospheres. In this study, high-resolution infrared spectra of H_2O broadened by CO_2 were recorded using a Fourier Transform Spectrometer in the 1.18 and 2.34 μm spectral regions. CO_2-collisional parameters for selected H_2O transitions were derived through a multispectrum fitting procedure employing both Voigt and quadratic speed-dependent Voigt profiles. Furthermore, calculations based on the semi-classical Complex Robert-Bonamy-Ma formalism were performed to estimate CO_2-broadened half-widths, line shifts, and their temperature dependencies across various atmospheric transparency windows. It results in a strong agreement between theoretical predictions and experimental data. Finally, the shared calculated linelist, obtained for a wide range of transitions, can be directly applied to radiative transfer modeling of atmospheres primarily composed of carbon dioxide.

Introduction

In the coming decade, several space missions are set to explore Venus' atmosphere, surface, and evolutionary history, relying on increasingly advanced instrumentation [1–3,4]. These missions aim to better characterize trace species such as water vapor, a key element to determine the D/H isotopic ratio and gaining deeper insights into planetary evolution processes [5–9,10]. To achieve this, radiative transfer models must rely on accurate spectroscopic parameters to enable robust atmospheric retrievals. However, concerning water vapor, most radiative transfer models use the air-collisional parameters instead of the CO_2-collisional parameters for H_2O lines, because of the lack of CO_2-collisional data [11].

To overcome this lack, since 1995 [12] several studies performed measurements of CO_2-collisional parameters for H_2O lines across various spectral regions [12–22,23]. Some of them include theoretical calculations, needed for atmospheric retrieval, as the laboratory measurements cannot cover all transitions of the spectral windows of interest for planetary studies.

Among these efforts, Régalia et al. (2019) [16] proposed a calculated linelist of H_2O lines broadened by CO_2 between 1300 and 5000 cm^{-1}. Nonetheless, several spectral regions relevant to Venus' atmosphere remain outside this range. Additional measurements and calculations are therefore required, particularly in the planet's main infrared transparency windows [24–27,28], where new experimental data can support further refinement of theoretical predictions.

In this context, new H_2O spectra broadened by CO_2 have been recorded using a high-resolution Fourier Transform Spectrometer (FTS) in two key spectral regions of atmospheric interest for Venus: 2.34 μm (from 3978 to 4306 cm^{-1}) and 1.18 μm (from 8486 to 8801 cm^{-1}), with the aim to determine accurate CO_2-collisional parameters for H_2O lines. Then, thanks to them, new calculations have been made to reach a wider number of H_2O transitions in the main Venusian infrared transparency windows.

First of all, Section 2 describes the experimental conditions to record H_2O broadened by CO_2 spectra around 1.18 and 2.34 μm. Section 3 presents the fitting procedure using two different line profiles and a comparison with the literature. Finally, new measured CO_2-collisional parameters are compared with new calculated ones based on the semi-classical Complex Robert-Bonamy-Ma formalism in Section 4.

* Corresponding author.
E-mail address: laurence.regalia@univ-reims.fr (L. Régalia).

https://doi.org/10.1016/j.jqsrt.2025.109576
Received 1 April 2025; Received in revised form 27 June 2025; Accepted 2 July 2025
Available online 7 July 2025

Experimental conditions

2.1. Experimental setup

Using a Bruker IFS 125HR Fourier Transform Spectrometer coupled with a 2-m White-type cell, new spectra of water vapor broadened by carbon dioxide were recorded in the 2.34 μm and 1.18 μm spectral regions, both being transparency windows for the Venusian atmosphere. The recording conditions are summarized in Table 1.

The multireflection cell is stainless-steel and can reach absorption path lengths from 8.262 to 104.262 m The pressure was monitored by three thermalized Leybold CTR101N Baratron gauges heads calibrated beforehand, according to measure ranges of 10, 100 and 1000 Torr and having an accuracy of 0.2 %. Four TGSA Pt100 probes with an accuracy of 0.6 K were used for the temperature monitoring.

The spectrometer and the reactor were put under vacuum using a primary oil pump and a secondary turbomolecular pump. For the rest of the experiment, the secondary pump maintained the spectrometer under a pressure of 1.10^{-4} mbar to reduce residual background water on the absorption path. An "empty cell" spectrum was recorded before each measurement and used to normalize the spectrum with absorbing gas.

2.2. Experimental method of gas injection

The experimental method is the same as the one used in Ref. [21]. After pumping over liquid water in natural abundance, water vapor was injected at low pressure to neglect, as much as possible, the contribution of the self-broadening coefficients. After H_2O pressure stabilization, CO_2 from Air Liquid with a stated purity (CO_2 N48) of 99.998 % was added into the gas cell. The CO_2 injection was repeated to reach different pressures from 100 to 500 Torr in the two spectral regions of interest.

The experimental conditions are listed in Table 2 and the different spectra of both spectral regions are presented in Figs. 1 and 2. Notice that at 1.18 μm, despite the increase of the absorption path length, most of the lines have an absorption not reaching 60 %, whereas at 2.34 μm, they are mostly upper than 30 %.

The H_2O partial pressure was measured using Baratron gauge heads after the single H_2O injection, while the CO_2 partial pressure was determined from the total pressure measured by the same gauges after each CO_2 injection. The temperature was averaged over the entire measurement duration. Moreover, the mean signal-to-noise ratio (SNR) was calculated using Bruker's software by selecting several spectral windows (approximately 3 cm^{-1} wide) where there are no absorption lines. The resulting SNR values reached 8300 and 6200 for the 2.34 μm and 1.18 μm spectral regions, respectively.

Table 1
Recording conditions of the infrared Fourier Transform Spectrometer and the multi-reflection gas cell used for measurements in the 2.34 μm and 1.18 μm spectral regions (corresponding to approximately 4273 cm^{-1} and 8475 cm^{-1}, respectively).

Infrared Fourier Transform Spectrometer		
Spectral region	2.34 μm	1.18 μm
Source	Tungsten	Tungsten
Iris radius	0.85 mm	1 mm
Focal length	418 mm	418 mm
Modulation frequency	40 kHz	60 kHz
Optical filter	Band pass 3750–4900 cm^{-1}	Band pass 7750–8900 cm^{-1}
Beam splitter	CaF_2	CaF_2
Detector	InSb, 77 K	InSb, 77 K
Maximum path difference	90 cm	45 cm
Spectral resolution (Bruker)	0.01 cm^{-1}	0.02 cm^{-1}
2-meter White Cell		
Absorption path length	64.262 m	104.262 m
Measurable line intensity range	2.10^{-24} to 7.10^{-22} cm^{-1} / (molecule.cm^{-2})	1.10^{-24} to 9.10^{-22} cm^{-1} / (molecule.cm^{-2})

Table 2
Experimental conditions for the eight H_2O-CO_2 spectra recorded in 2.34 μm and 1.18 μm spectral regions at room temperature. The second and third columns present the fitted H_2O partial pressure determined using MFT [29], and the relative deviation obtained by comparing the fitted values with those measured by the Baratron gauges, calculated as (fitted H_2O pressure - measured H_2O pressure)/measured H_2O pressure.

Measured H_2O partial pressure [Torr]	Fitted H_2O partial pressure [Torr]	Relative deviation [%]	CO_2 partial pressure [Torr]	Temperature [K]
Spectral region 2.34 μm				
0.982	0.940	−4.3	101.4	296.9
0.982	0.932	−5.1	202.1	296.9
0.982	0.925	−5.8	302.6	296.8
0.982	0.920	−6.3	500.5	296.8
Spectral region 1.18 μm				
0.999	0.895	−10.4	100.7	295.1
0.999	0.874	−12.5	207.3	294.9
0.999	0.865	−13.4	301.2	294.9
0.999	0.855	−14.4	501.0	294.9

2.3. H_2O partial pressure

As explained and detailed in our previous article [21], the injection of a polar molecule, like H_2O, in a stainless-steel reactor can lead to adsorption effects that have an impact on the water vapor partial pressure value in the cell. To take into account this phenomenon, the multispectrum fitting program MultiFiT [29] (MFT) was used to fit H_2O partial pressure for each spectrum. The intensity parameters, which have to be as accurate as possible, were fixed to the HITRAN2020 values [30] during the multispectrum fitting process. In the 2.34 μm spectral region, 8 water lines measured by Loos et al. (2017) [31], having an uncertainty on the line intensity parameter <1 % [30], were used to ensure an accurate determination of the H_2O partial pressure. While, in the 1.18 μm spectral region, 19 water lines calculated by Conway et al. (2020) [32] with an uncertainty on the line intensity parameter between 2 and 5 % [30] were used, leading to less precise determination of the partial pressure of H_2O. The relative deviation between measured and fitted H_2O partial pressure is shown in Table 2 and is calculated as follows: (fitted H_2O pressure - measured H_2O pressure)/measured H_2O pressure. Note that the fitted H_2O partial pressures reflect the best agreement with the observed line intensities, minimizing residuals and implicitly accounting as best as possible for possible water vapor adsorption effects in the experimental cell. The difference in relative deviations between the two spectral regions may partly result from the different origins of the used HITRAN line intensities. As mentioned above, despite the increased absorption path length at 1.18 μm, most lines exhibit absorption levels not exceeding 60 %, unlike at 2.34 μm. This difference may also have affected the H_2O partial pressure retrieval, as weak and strong absorption lines do not respond in the same way. Furthermore, as also shown by Gamache et al. (2023) [33] for H_2O broadened by O_2, the retrieved partial pressure of H_2O tends to decrease with increasing broadening gas pressure.

Line shape parameters determination

This section explains how the CO_2-collisional parameters for H_2O lines were determined from the recorded spectra using a multispectrum fitting procedure with different line profiles. The multispectrum fitting procedure will be presented in the following section before a discussion on the fitting residuals obtained with two different line profiles.

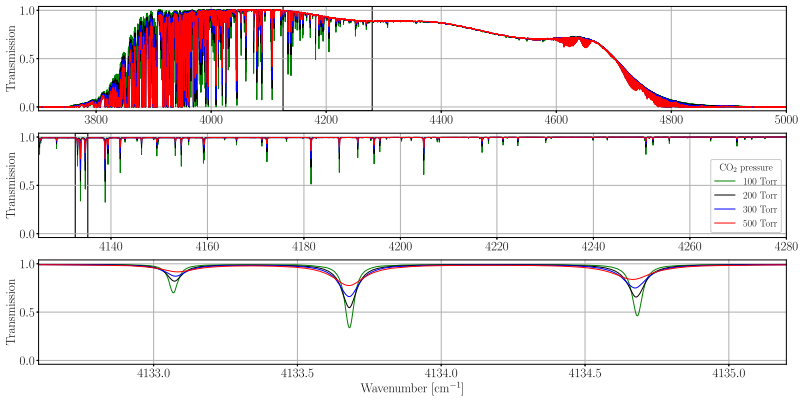

Fig. 1. Four spectra of water vapor broadened by carbon dioxide measured in the 2.34 μm spectral region in the upper panel. Two successive zooms on a few H_2O lines are represented in the middle and lowest panel.

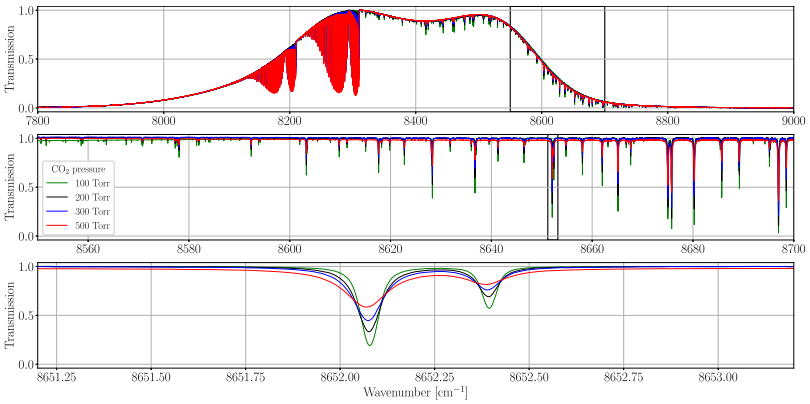

Fig. 2. Four spectra of water vapor broadened by carbon dioxide measured in the 1.18 μm spectral region, with two successive zooms on a few H_2O lines, from top to bottom panels.

3.1. *Multispectrum fitting procedure*

For both spectral regions, isolated H_2O lines with an absorption range from 10 % to 80 % were selected to obtain accurate line-shape parameters. The MultiSpectrum Fitting (MSF) [34] program based on the least squares method was used to determine the CO_2-collisional parameters for some H_2O rovibrational transitions in different spectral bands, employing different line profiles. Some of them were used in Ref. [21], but the most coherent for the H_2O-CO_2 collision system in these experimental conditions were the Voigt [35] and the quadratic Speed-Dependent Voigt (qSDV) [36–38,39] profiles. The first is generally implemented in models for its simplicity (a convolution between a Gaussian profile and a Lorentz profile) and its low number of parameters (the pressure-induced broadening Γ_0 and shift Δ_0 coefficients). However, it can result in significant residuals, often referred to as a "W-shape". This phenomenon arises from line narrowing, which the Voigt profile does not account for; it also happens due to speed dependence. To mitigate the discrepancy between measurements and fits, the qSDV profile can be used to take into account the speed dependence of the collisional parameters. It is defined by two additional parameters compared to the Voigt profile, Γ_2 the speed-dependence of the pressure-induced broadening coefficient and Δ_2 the speed-dependence of the pressure-induced shift coefficient.

As we determined the H_2O partial pressure by fixing the intensity values to those from HITRAN2020 [30], these values were kept fixed during the fitting process of the collisional parameters. Throughout the multispectrum fitting procedure the position, broadening, and shift coefficients were allowed to vary simultaneously. Specifically, when using the qSDV profile, the speed-dependences of the broadening and shift coefficients were also fitted.

The apparatus function was taken into account during the fitting process. The width of the instrumental line shape was chosen near the Doppler width of H_2O at the studied wavelength. Under these conditions, the apparatus function has no significant influence on the CO_2-broadened spectra. Consequently, its impact on the determination of the collisional parameters is negligible.

Finally, it is important to notice that the MFT program [29], mentioned earlier, was limited to the Voigt profile and thus was exclusively used for the H_2O partial pressure fit.

3.2. *Line profile comparison*

Figs. 3 and 4 compare the fits obtained using the Voigt profile and the qSDV profile in the two analyzed spectral regions.

In Fig. 3, the Voigt fitting residuals exhibit the characteristic W-shape, which is significantly reduced using the qSDV profile, as what has already been observed in Ref. [21]. In Fig. 4, the residuals from the Voigt profile are lower and further reduced by accounting for speed dependence effects. Regarding the CO_2-broadening coefficient Γ_0 values obtained with both profiles, Γ_0 (qSDV) is consistently larger than Γ_0 (Voigt) with a mean increase of 4.9 %. This is coherent with the 4.1 % increase found at 2.7 μm in Ref. [21].

Therefore, by incorporating speed-dependence effects, the experimental line-shape is better reproduced, achieving fitting residuals below 0.1 %. This enhancement is essential for obtaining reliable CO_2-collisional parameters, which will be increasingly crucial for high-precision atmospheric modeling as space instruments continue to improve.

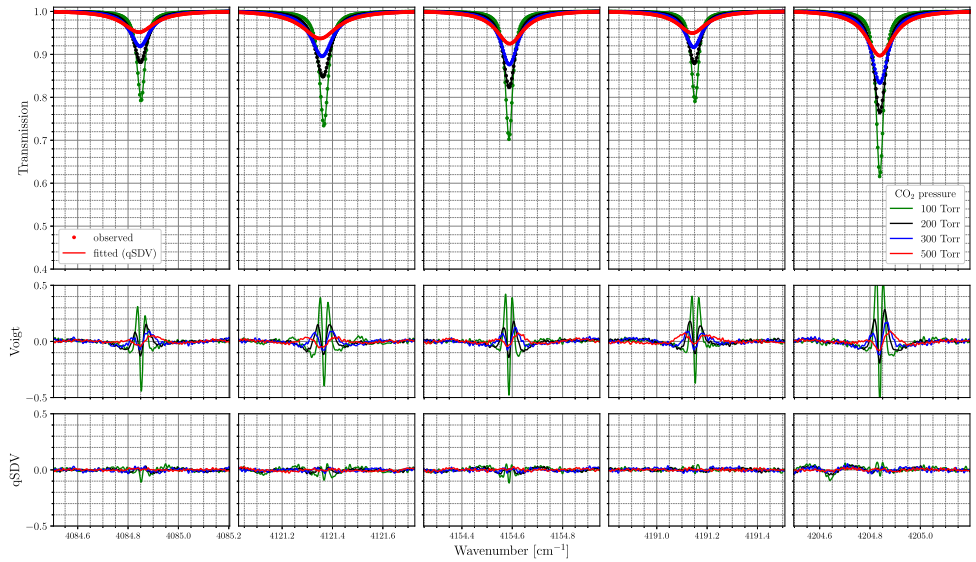

Fig. 3. Example of five H_2O spectral lines broadened by different CO_2 partial pressures in the 2.34 μm spectral region fitted with the Voigt and the quadratic speed-dependent Voigt profiles. The first row presents the observed and qSDV fitted water vapor line transmission. The second and third rows show respectively the Voigt and the quadratic speed-dependent Voigt fitting residuals in percentage, calculated as 100 x (Obs.-Calc.).

Fig. 4. Example of five H_2O spectral lines broadened by different CO_2 partial pressures in the 1.18 μm spectral region fitted with the Voigt and the quadratic speed-dependent Voigt profiles. The first row presents the observed and qSDV fitted water vapor line transmission. The second and third rows show respectively the Voigt and the quadratic speed-dependent Voigt fitting residuals in percentage, calculated as 100 x (Obs.-Calc.).

3.3. Literature comparison

In the literature, previous qSDV CO_2-collisional parameters for water vapor lines were recently measured by Deichuli et al. [17]. However, the number of comparable transitions remains limited (Fig. 5) due to differences in experimental setups — notably, their measurements were performed using only one single-pass cell with a 24 cm path length. For the collisional half-widths obtained with qSDV, a mean relative deviation of 3.3 % is observed, with a standard deviation of 6.5 %, indicating a reasonably good agreement with our results, as shown on the bottom left panel of Fig. 5. In contrast, the comparison of the speed-dependence parameters of the half-widths shows a larger mean relative deviation of 27.2 %, with a standard deviation of 69.1 %, as seen on the bottom right panel of Fig. 5. This significant dispersion highlights the greater sensitivity of speed-dependent parameters to experimental conditions such as signal-to-noise ratio, spectral resolution, line selection, and pressure range. Using a wide range of CO_2 pressures allows for a large variation in the ratio between the Lorentz and Doppler widths, which improves the fit quality and facilitates the retrieval of higher-order collisional parameters such as Γ_2 and Δ_2, as discussed in Ngo et al. (2013) [39]. Moreover, the experimental setup in Deichuli et al. [17] was more restrictive: the absorption cell was significantly shorter, limiting access to the same H_2O transitions. The few lines available for comparison correspond to the weakest absorption lines in Ref. [17]. For these lines the determination of collisional parameters—especially the higher-order ones—is more sensitive to experimental conditions and prone to dispersion. Indeed, extracting accurate speed-dependence coefficients requires very high-quality spectra and precise control of experimental parameters, which can be difficult to achieve in practice, especially for H_2O due to adsorption phenomena. These results underline the need for improvements in experimental conditions to better constrain these sensitive parameters. The comparison of the shift coefficient and its

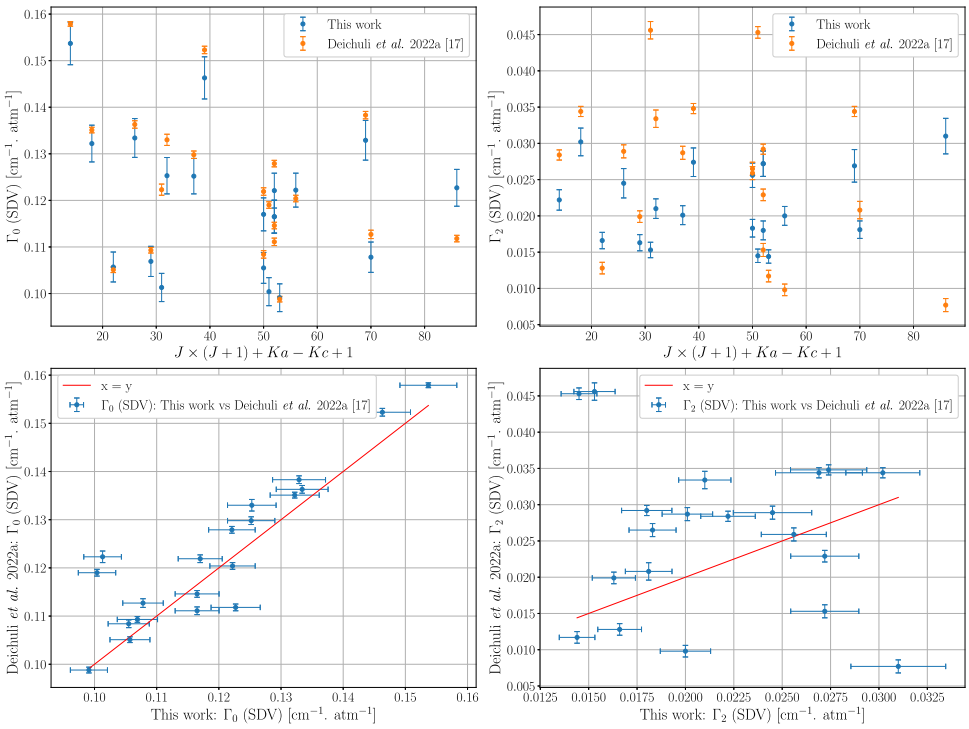

Fig. 5. Top left panel, a comparison is shown between the CO_2-broadening coefficients Γ_0 from this study at 2.34 μm and those from Deichuli et al. [17] for 20 common water lines. The 1-σ error bars of the broadening coefficients of this work consider the numerical uncertainties, which are very small, and the experimental uncertainties, estimated at 2 %, coming mainly from the fit of water vapor partial pressure. Top right panel, a similar comparison is presented for Γ_2, the speed-dependence of the CO_2-broadening parameters, where the experimental uncertainties are estimated at 5 % in addition to numerical uncertainties. Note that for Deichuli et al. parameters, only the 1-σ numerical uncertainties are shown. The bottom panels show the correlation between this work and the literature for Γ_0 and Γ_2 collisional parameters obtained using a speed-dependent Voigt profile.

speed-dependence is not possible with our values because the second one was fixed to zero in Deichuli et al. [17], as mentioned in our previous article [21]. To further assess the impact of this Δ_2 parameter, additional tests were performed with Δ_2 fixed to zero. This led to a mean relative difference of 2.1 % with a standard deviation of 3.7 % for the broadening parameters, and respectively 12.2 % and 28.5 % for their speed-dependence — suggesting, at first glance, a better agreement with the data from [17]. However, the fitting residuals showed larger deviations and a poorer overall fit, confirming that including Δ_2 gives a better and more reliable fit to the line shapes.

New line lists

After the description of the new experimental line list at the beginning of this section, the theoretical model based on a semi-classical Complex Robert-Bonamy-Ma formalism is presented. The results of the calculations are then compared with the experimental values.

4.1. Experimental line list

Thanks to the fitted H_2O partial pressure values and the program MSF [34], CO_2-collisional parameters were determined for 60 rovibrational $H_2^{16}O$ transitions in the 2.34 μm spectral region and 65 transitions in the 1.18 μm region. These new results were combined with data at 2.7 μm, previously measured and presented in [21]. A total of 187 CO_2-broadening and shift coefficients for water lines using the Voigt profile was obtained. Moreover, for 106 of these lines, the speed dependence of the CO_2-broadening and shift coefficients was considered using the quadratic speed-dependent Voigt profile. The vibrational bands probed are detailed in Table 3. The measured H_2O-CO_2 collisional parameters are available in the supplementary materials in three different files corresponding to each studied spectral region.

Table 3
Number of measured $H_2^{16}O$ transitions broadened by carbon dioxide in each observed vibrational band.

Band	Number of $H_2^{16}O$ fitted transitions
Spectral region: 2.7 μm	
0 0 1 ← 0 0 0	29
1 0 0 ← 0 0 0	15
0 2 0 ← 0 0 0	18
Spectral region: 2.34 μm	
0 0 1 ← 0 0 0	39
1 0 0 ← 0 0 0	21
Spectral region: 1.18 μm	
1 1 1 ← 0 0 0	53
0 3 1 ← 0 0 0	8
2 1 0 ← 0 0 0	3
1 3 0 ← 0 0 0	1
TOTAL	187

Concerning the uncertainty on the newly measured CO_2-collisional parameters, several sources can contribute: the instrumental line shape, the absorption path length, the temperature measurement, the determination of CO_2 and H_2O partial pressures, and the use of the multi-spectrum fitting procedure. The instrumental function has a negligible effect on the final uncertainty, as its width is much smaller than the collisional broadening. Similarly, the absorption path length and cell temperature are well characterized and stable. Regarding the CO_2 partial pressure, since CO_2 does not adsorb onto the cell walls, its measurement is considered reliable, and thus its effect on the collisional parameters' uncertainty is minimal.

The main sources of uncertainty on the CO_2-collisional parameters are (1) the numerical uncertainty from the multi-spectrum fitting procedure and (2) the uncertainty on the retrieved water vapor partial pressure, which is directly linked to the uncertainty in the H_2O line

intensities used in the retrieval. The total uncertainty is therefore the sum of these two contributions. A 1 % uncertainty in the H_2O line intensities translates to a 1 % uncertainty in the retrieved water vapor partial pressure, which in turn leads to an approximately 1 % uncertainty on the broadening parameter. The uncertainty on the shift parameter was estimated as higher than that of the broadening uncertainty, as these parameters are more difficult to measure, with a maximum uncertainty set to 5 %. For the speed-dependence coefficients, the uncertainty was estimated at 5 %. When the H_2O line intensities originated from Loos et al. (2017) [31], an additional 1 % uncertainty was added to account for the fact that those intensities were scaled on experimental data using a speed-dependent Voigt profile, whereas a standard Voigt profile was used in the water vapor partial pressure fit. The estimated uncertainties for each collisional parameter and spectral region are provided in the readme file included in the supplementary materials.

4.2. CRBM calculations

The line shape parameters were calculated using the semi-classical Complex Robert-Bonamy-Ma (CRBM) formalism [40,41]. The half-width and line shift of a given ro-vibrational transition $f \leftarrow i$ are given by the real and imaginary components of the following expression:

$$(\gamma - i\delta)_{f\leftarrow i} = \frac{n_2}{2\pi c}\int_0^\infty v \times f(v)\, dv \int_0^\infty 2\pi b\, db \times \left[1 - e^{-i\langle S_1 + \mathrm{Im}\{S_2\}\rangle_{J_2}}\; e^{\langle -\mathrm{Re}\{S_2\}\rangle_{J_2}}\right] \quad (1)$$

where n_2 is the density number of perturber, c the speed of light, $f(v)$ the Maxwell-Boltzmann distribution of the velocity v, b is the impact parameter, S_1 and S_2 are the first and second orders of the successive expansion of the scattering matrix [42,43]. The S_1 and S_2 terms depend on the ro-vibrational states of the optical transition, on the associated collisionally induced transitions from these states, on the intermolecular potential, and on the collision dynamic. The semi-classical formulation refers to the fact that the trajectory of the colliding molecule is treated using classical mechanics while the internal structure of the molecules (both radiator and perturber) is treated quantum mechanically. The active molecule of an optical transition from $f \leftarrow i$ will undergo collisions with the bath of perturber molecules. These collisions will induce non-radiative transitions of the initial (i) and final (f) states of the radiating molecule to states i' and f' interrupting the radiation and causing collisional broadening and shifting. The prime states are called *collisionally connected states* and are given by selection rules determined by the wavefunctions and the intermolecular potential. Since the high-order intermolecular potential contains a lot of terms, many i' and f' are possible. The quantum mechanical components of the calculations are the energy of the states involved in the non-radiative transitions and the wavefunctions of the states which are used to determine the probability of the collisionally induced transition through the reduced matrix elements (RME). A recent study [44] showed that CRBM calculations should use the ground state RMEs for all vibrational states to ensure completeness.

The intermolecular potential used in the calculation was composed of electrostatic terms, atom-atom components and the induction and London dispersion terms. The atom-atom components are expanded to the 20th *order* and *rank* 4 to ensure convergence. The atom-atom part of the potential was determined to reproduce the half-width measured in the ν_2 band of H_2O diluted in CO_2 by Brown et al. [13] and Régalia et al. [16]. The methodology has been previously explained and has shown to provide excellent results [45–47]. The atom-atom components of the final potential are given in Table 4 and reproduced the ν_2 band data of Brown et al. [13] and Régalia et al. [16] with an Average Percent Difference of −1.57 % and −0.08 % and standard deviation of 5.75 % and 5.25 %, respectively. All other parameters are set to the literature recommended values: the dipole moment of water vapor and its vibrational dependence are taken from Shostak and Muenter [48], the quadrupole moments are from Flygare and Benson [49]. The polarizability and its vibrational dependence come from Luo et al. [50]. The vibrationally-independent ionization potential is taken from [51]. For carbon dioxide, the quadrupole moment is taken out of Chetty and Couling [52], the polarizability from Bogaard and Orr [53] and the ionization potential from Tanaka et al. [54].

Table 4
Final atom-atom constants for the H_2O-CO_2 collision system.

Atom-atom	ε/k [K]	σ [Å]
H-O	21.717	3.2798
H-C	18.470	3.1100
O-O	51.730	4.0635
O-C	60.550	3.0000

The speed-dependences of the line shape parameters are given by two parameters representing the line broadening, (γ_0, γ_2), and two parameters representing the line shift, (δ_0, δ_2). γ_0 and δ_0 are, respectively, the collisional width and shift averaged over all speeds, while γ_2 and δ_2 are the quadratic terms describing the speed dependence of the broadening and shift [55,56] as shown in Eqs. (2).

$$\gamma(v_a) = \gamma_0 + \gamma_2\left[\left(\frac{v_a}{v_{a_0}}\right)^2 - \frac{3}{2}\right] \quad (2a)$$

$$\delta(v_a) = \delta_0 + \delta_2\left[\left(\frac{v_a}{v_{a_0}}\right)^2 - \frac{3}{2}\right] \quad (2b)$$

where v_a is the speed of the active-molecule and v_{a0} is its most probable speed.

Calculating the integral over db in Eq. (1) gives the collisional cross-sections as a function of the relative velocity,

$$(\sigma_{\mathrm{Re}}(v_{rel}) - i\sigma_{\mathrm{Im}}(v_{rel})) = \int_0^\infty 2\pi b\, db\left[1 - e^{-i\langle S_1 + \mathrm{Im}\{S_2\}\rangle_{J_2}}\; e^{\langle -\mathrm{Re}\{S_2\}\rangle_{J_2}}\right] \quad (3)$$

and allows the determination of the half-width and line shift as a function of v_{rel}

$$\gamma_{f\leftarrow i}(v_{rel}) + i\delta_{f\leftarrow i}(v_{rel}) = \frac{n_2}{2\pi c} v_{rel}[\sigma_{\mathrm{Re}}(v_{rel}) + i\sigma_{\mathrm{Im}}(v_{rel})] \quad (4)$$

Given $\gamma(v_{rel})$ and $\delta(v_{rel})$ the half-width and line shift as a function of the absolute speed of the active molecule [37,38,57,58], v_a, allowing a fit to be made to the data to determine the speed dependence of the half-width and line shift. These calculations will be part of the future work.

The CRBM calculations include all real and imaginary terms allowing the determination of the half-width and line shift from a single calculation. The RMEs were determined from *ab initio* wavefunctions following Lamouroux et al. [59]. The trajectories are deduced from Hamilton's equations and an explicit velocity averaging over the Boltzmann distribution was done.

4.3. Measured vs calculated parameters comparison

Thanks to the improvements made to the H_2O-CO_2 molecular potential, the calculation of spectroscopic parameters for this collision system has become more accurate. Comparisons between the most recent experimental H_2O-CO_2 spectroscopic parameters and the newly calculated ones are presented for the 2.7 μm, 2.34 μm, and 1.18 μm spectral regions, as shown in Figs. 6, 7, and 8, respectively. As the most common line profile in the study of the radiative transfer of planetary atmospheres remains the Voigt profile, the comparison between measured and calculated parameters was made on parameters coming from Voigt profile. Table 5 highlights the resulting deviations, which are notably low, indicating a very good agreement between the

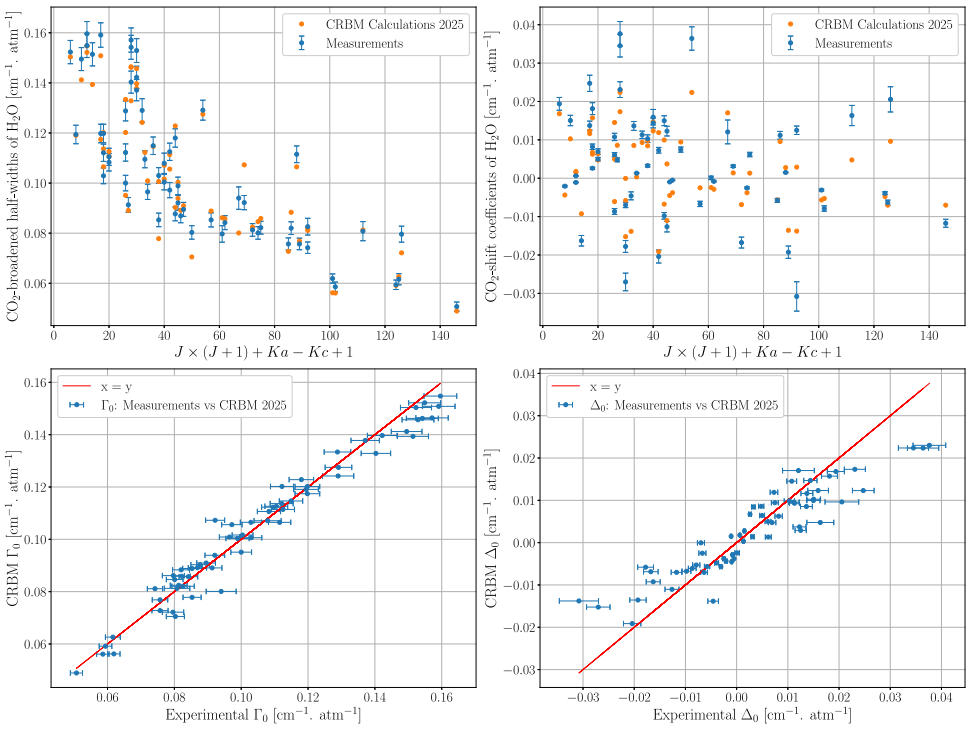

Fig. 6. On top panels: comparison between measured and calculated CO_2-broadening (Γ_0) and shift (Δ_0) coefficients for some water transitions in the 2.7 μm spectral region coming from Ducreux et al. (2024) [21]. The uncertainties at 1-σ came from numerical errors provided by the multi-spectrum fitting procedure and mainly from H_2O partial pressure error. This last one is estimated at 2 % for the half-widths and 3 % for the shifts. On bottom panels: correlation plots between measurements, obtained using a Voigt profile, and calculations for Γ_0 and Δ_0 collisional parameters.

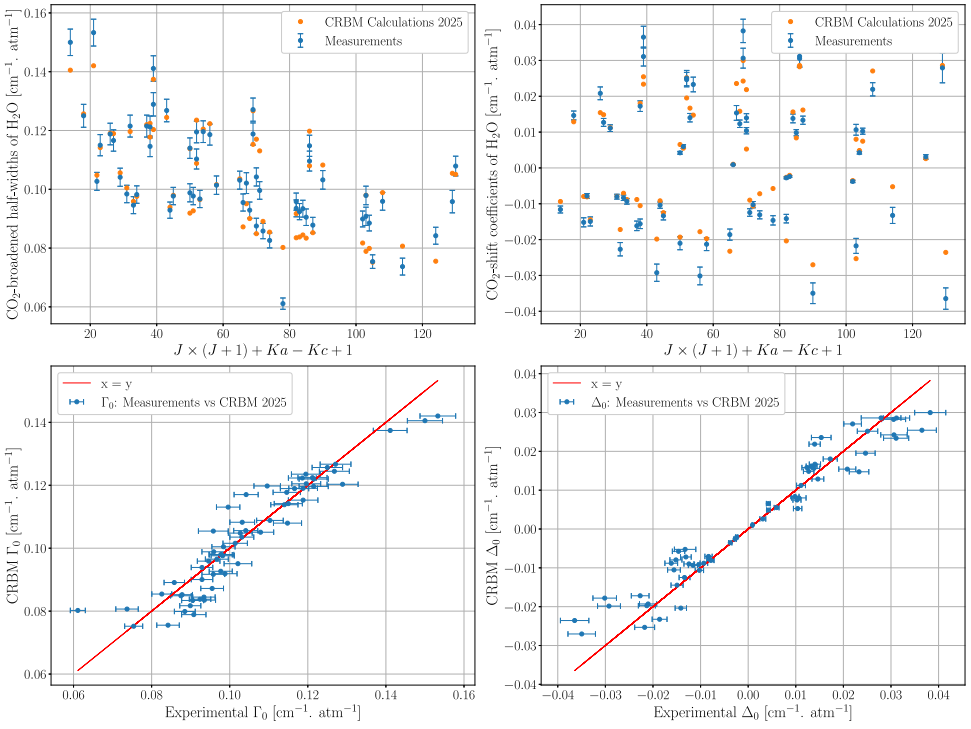

Fig. 7. On top panels: comparison between measured and calculated CO_2-broadening (Γ_0) and shift (Δ_0) coefficients for some water transitions in the 2.34 μm spectral region. The uncertainties at 1-σ came from numerical errors provided by the multi-spectrum fitting procedure and mainly from H_2O partial pressure error. This last one is estimated at 2 % for the half-widths and 3 % for the shifts. On bottom panels: correlation plots between measurements, obtained using a Voigt profile, and calculations for Γ_0 and Δ_0 collisional parameters.

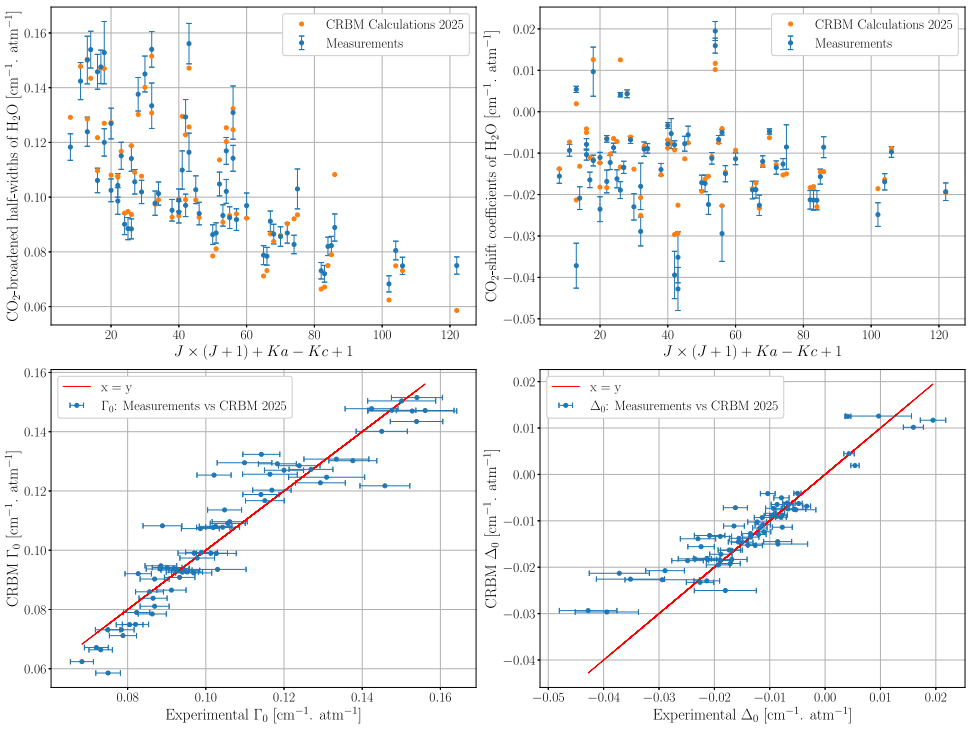

Fig. 8. On top panels: comparison between measured and calculated CO_2-broadening (Γ_0) and shift (Δ_0) coefficients for some water transitions in the 1.18 μm spectral region. The uncertainties at 1-σ came from numerical errors provided by the multi-spectrum fitting procedure and mainly from H_2O partial pressure error. This last one is estimated at 3 % for the half-widths and 5 % for the shifts. On bottom panels: correlation plots between measurements, obtained using a Voigt profile, and calculations for Γ_0 and Δ_0 collisional parameters.

Table 5
Deviations between measurements and calculations in three spectral regions on CO_2-broadening and shift parameters for H_2O lines. APD is the Average in Percent Deviation calculated as the mean of (calculated parameter - experimental parameter) / experimental parameter. The mean absolute deviation is calculated as the mean of |calculated parameter - experimental parameter| / experimental parameter and SD is the standard deviation.

Spectral region [μm]	CO_2-broadened half-width of H_2O lines			CO_2-shift coefficient of H_2O lines			Number of compared H_2O lines
	APD [%]	Mean absolute deviation [%]	SD [%]	Average deviation [cm^{-1}. atm^{-1}]	Mean absolute deviation [cm^{-1}.atm^{-1}]	SD [cm^{-1}. atm^{-1}]	
2.7	−0.4	4.1	5.4	-0.7×10^{-3}	4.8×10^{-3}	6.2×10^{-3}	62
2.34	−0.6	4.8	7.0	0.9×10^{-3}	3.8×10^{-3}	5.1×10^{-3}	60
1.18	0.1	6.0	7.9	1.6×10^{-3}	3.6×10^{-3}	4.8×10^{-3}	65

experimental measurements and the calculations using the updated molecular potential. In addition, correlation plots on Figs. 6, 7, and 8 underline the consistency of the measurements, especially for the pressure-induced shift parameters which are complex to determine and depend a lot on experimental conditions.

Using the determined intermolecular potential, CRBM calculations were performed, at 13 temperatures between 200 and 3000 K, for transitions of the 3 main isotoplogues of water vapor having an intensity larger 10^{-28} $cm^{-1}/(mol.cm^{-2})$ and belonging to the main Venusian infrared transparency windows. The temperature dependencies of the line shape parameters were determined using the standard power law, $\gamma(T) = \gamma(T_0)\ (T_0/T)^n$, for addition to the HITRAN format file. The temperature dependence determined using the second order approximation of the Gamache-Vispoel temperature dependence law [60] were also computed and are available from the corresponding author. These data were not added to the line file as the simulation code currently only uses the standard power law data. The temperature dependencies of the line shape parameters were determined using the empirical power law. The computed line shape information was incorporated in a HITRAN-like file using the "diet" scheme [61]: for a particular rovibrational transition. First, if measurement data are available, they were used. Next if a CRBM calculation was made, these data were used. Next, if available, data computed for a transition having the same rotation quantum number were used (i.e. vibrational dependence is ignored). Finally, if measurement and calculations are not available for the transition, a J"-averaged value is used. Note that in the two last cases, the line shift is set to zero. Line shape information for HDO perturbed by CO_2 was also included using the results of Malathy Devi et al. [62,63], only the D_2O isotopologue was not considered. The generated linelist is available in the supplementary materials.

4.3.1. *Vibrational dependence of the half-widths*

Using the datasets of 4535 calculations and 525 measured of the half-width for 41 vibrational states: 17 cold bands (transitions originating from the ground vibrational state (000)) and 24 hot bands (lower state is not the ground vibrational state (000)), the vibrational dependence of the half-width was studied. For a given set of rotational quantum numbers, the average percent difference (APD), absolute average percent difference (AAPD) and standard deviation (SD) in percent was determined. This procedure gave 589 APDs, and 292 AAPDs and SDs, implying 297 of the comparisons were for 2 data points. Then the same statistical quantities were determined for the APDs, AAPDs, and SDs of the comparisons. Table 6 gives the statistics of comparing APDs, AAPDs, and SDs of the comparisons, i.e. vibrational dependence of g. The data

Table 6
Statistics of the vibrational dependence of the half-width, Given are the number of comparisons, the average percent difference of the APDs, the average absolute percent difference of the AAPDs and the average standard deviation in percent of the SDs.

Quantity	# comparisons	Average % difference	Average absolute % difference	Average standard deviation
APDs	589	−0.16765	3.07395	6.02916
AAPDs	292	3.60597	3.60597	2.87653
SDs	292	3.56223	3.56224	3.22872

show that the vibrational dependence of the half-width is small, −0.168 % on average with the AAPD and SD roughly 3–4 %.

Conclusion

The newly measured H_2O broadened by CO_2 collisional parameters, obtained using an infrared Fourier Transform Spectrometer and a multispectrum fitting approach, show excellent consistency with CRBM calculations based on a refined intermolecular potential for the H_2O-CO_2 system. This agreement highlights the strength and predictive capability of theoretical models, especially in spectral regions where experimental measurements are limited by different factors such as limited optical path lengths, restricted pressure ranges, and line overlapping. The consistency between measured and calculated parameters, particularly for the pressure shift coefficients, which are challenging to measure, reinforces the reliability of the dataset and supports its use in atmospheric studies.

This dataset of line-shape parameters for H_2O broadened by CO_2 provides a valuable resource for atmospheric radiative transfer modeling in CO_2-rich planetary environments. By combining the present results with the earlier work of Régalia et al. (2019) [16], these linelists serve as an important spectroscopic reference for modeling H_2O absorption in planetary atmospheres such as those of Venus, Mars, and certain exoplanets. Finally, the experimental and calculated linelists of H_2O broadened by CO_2 line-shape parameters are available in the supplementary materials.

Given the increasing capabilities of future planetary missions, these high-precision data are essential for advancing the accuracy of atmospheric property retrievals. Another article is being written to show the impact of these collisional parameters on atmospheric planetary retrievals.

CRediT authorship contribution statement

É. Ducreux: Writing – original draft, Software, Formal analysis, Data curation. **B. Vispoel:** Writing – original draft, Resources, Investigation, Data curation. **B. Grouiez:** Writing – review & editing, Data curation. **R. R. Gamache:** Writing – review & editing, Supervision, Methodology, Formal analysis, Data curation. **M. Lepère:** Writing – review & editing, Supervision. **S. Robert:** Writing – review & editing, Supervision, Project administration. **L. Régalia:** Writing – original draft, Validation, Supervision, Methodology, Funding acquisition.

Declaration of competing interest

The authors declare that they have no known competing financial interests or personal relationships that could have appeared to influence the work reported in this paper.

Acknowledgements

This work was supported by the Programme National de Planétologie (PNP) of CNRS-INSU co-funded by CNES. S.R. acknowledges funding by the Belgian Science Policy Office (BELSPO) through the FED-tWIN program (Prf-2019–077 - RT-MOLEXO) and through financial and contractual support coordinated by the ESA Prodex Office (PEA 4000137943, 4000128137). B.V. would like to thank the F.R.S.-FNRS for postdoctoral financial support.

Supplementary materials

Supplementary material associated with this article can be found, in the online version, at doi:10.1016/j.jqsrt.2025.109576.

Data availability

Data will be available in supplementary materials.

References

[1] Neefs E, Vandaele AC, De Cock R, Erwin J, Robert S, Thomas IR, et al. VenSpec-H spectrometer on the ESA EnVision mission: design, modeling, analysis. Acta Astronaut 2025;226:178–201. https://doi.org/10.1016/j.actaastro.2024.10.018.
[2] Widemann T, Smrekar SE, Garvin JB, Straume-Lindner AG, Ocampo AC, Schulte MD, et al. Venus Evolution through time: key science questions, selected mission concepts and future investigations. Space Sci Rev 2023;219:56. https://doi.org/10.1007/s11214-023-00992-w.
[3] Smrekar S, Hensley S, Nybakken R, Wallace MS, Perkovic-Martin D, You T-H, et al. VERITAS (Venus Emissivity, Radio Science, InSAR, Topography, and Spectroscopy): a Discovery mission. 2022. IEEE Aerosp Conf AERO 2022:1–20. https://doi.org/10.1109/AERO53065.2022.9843269.
[4] Garvin JB, Getty SA, Arney GN, Johnson NM, Kohler E, Schwer KO, et al. Revealing the mysteries of Venus: the DAVINCI Mission. Planet Sci J 2022;3:117. https://doi.org/10.3847/PSJ/ac63c2.
[5] Fedorova A, Korablev O, Vandaele A-C, Bertaux J-L, Belyaev D, Mahieux A, et al. HDO and H_2O vertical distributions and isotopic ratio in the Venus mesosphere by Solar Occultation at Infrared spectrometer on board Venus Express. J Geophys Res Planets 2008;113. https://doi.org/10.1029/2008JE003146.
[6] Krasnopolsky VA, Belyaev DA, Gordon IE, Li G, Rothman LS. Observations of D/H ratios in H_2O, HCl, and HF on Venus and new DCl and DF line strengths. Icarus 2013;224:57–65. https://doi.org/10.1016/j.icarus.2013.02.010.
[7] Villanueva GL, Mumma MJ, Novak RE, Käufl HU, Hartogh P, Encrenaz T, et al. Strong water isotopic anomalies in the martian atmosphere: probing current and ancient reservoirs. Science 2015;348:218–21. https://doi.org/10.1126/science.aaa3630.
[8] Villanueva GL, Liuzzi G, Aoki S, Stone SW, Brines A, Thomas IR, et al. The deuterium isotopic ratio of water released from the martian caps as measured with TGO/NOMAD. Geophys Res Lett 2022;49:e2022GL098161. https://doi.org/10.1029/2022GL098161.
[9] Vandaele AC, Korablev O, Daerden F, Aoki S, Thomas IR, Altieri F, et al. Martian dust storm impact on atmospheric H_2O and D/H observed by ExoMars Trace Gas Orbiter. Nature 2019;568:521–5. https://doi.org/10.1038/s41586-019-1097-3.
[10] Mahieux A, Viscardy S, Yelle RV, Karyu H, Chamberlain S, Robert S, et al. Unexpected increase of the deuterium to hydrogen ratio in the Venus mesosphere. Proc Natl Acad Sci 2024;121:e2401638121. https://doi.org/10.1073/pnas.2401638121.
[11] Jorge J, Wordsworth R, Adams D. Greenhouse warming potential of a suite of gas species on early Mars evaluated using a radiative-convective climate model. J Geophys Res Planets 2024;129:e2024JE008443. https://doi.org/10.1029/2024JE008443.
[12] Gamache RR, Neshyba SP, Plateaux JJ, Barbe A, Regalia L, Pollack JB. CO_2-Broadening of water-vapor lines. J Mol Spectrosc 1995;170:131–51. https://doi.org/10.1006/jmsp.1995.1060.
[13] Brown LR, Humphrey CM, Gamache RR. CO_2-broadened water in the pure rotation and ν_2 fundamental regions. J Mol Spectrosc 2007;246:1–21. https://doi.org/10.1016/j.jms.2007.07.010.
[14] Sagawa H, Mendrok J, Seta T, Hoshina H, Baron P, Suzuki K, et al. Pressure broadening coefficients of H_2O induced by CO_2 for Venus atmosphere. J Quant Spectrosc Radiat Transf 2009;110:2027–36. https://doi.org/10.1016/j.jqsrt.2009.05.003.
[15] Borkov YuG, Petrova TM, Solodov AM, Solodov AA. Measurements of the broadening and shift parameters of the water vapor spectral lines in the 10,100-10,800 cm^{-1} region induced by pressure of carbon dioxide. J Mol Spectrosc 2018;344:39–45. https://doi.org/10.1016/j.jms.2017.10.010.
[16] Régalia L, Cousin E, Gamache RR, Vispoel B, Robert S, Thomas X. Laboratory measurements and calculations of line shape parameters of the H_2O-CO_2 collision system. J Quant Spectrosc Radiat Transf 2019;231:126–35. https://doi.org/10.1016/j.jqsrt.2019.04.012.
[17] Deichuli VM, Petrova TM, Solodov AA, Solodov AM. Broadening and shift coefficients of water absorption lines induced by carbon dioxide pressure near 2.7 μm. Atmos Ocean Opt 2022;35:634–8. https://doi.org/10.1134/S1024856022060070.
[18] Deichuli VM, Petrova TM, Solodov AM, Solodov AA, Fedorova AA. Water vapor absorption line parameters in the 6760-7430 cm^{-1} region for application to CO_2-

rich planetary atmosphere. J Quant Spectrosc Radiat Transf 2022;293:108386. https://doi.org/10.1016/j.jqsrt.2022.108386.
[19] Yang T, Qian X-M, Ma H-L, Liu Q, Zhu, Zheng J-J, et al. CO_2-broadened coefficients of water vapor molecule in 1.1 μm band. Acta Phys Sin 2022;71:203301–7. https://doi.org/10.7498/aps.71.20220700.
[20] Petrova TM, Solodov AM, Solodov AA, Deichuli VM, Lavrentieva NN, Dudaryonok AS. Measurements and calculations of CO_2-broadening and shift coefficients of water vapor transitions in the 5150-5550 cm^{-1} spectral region. J Quant Spectrosc Radiat Transf 2023;311:108757. https://doi.org/10.1016/j.jqsrt.2023.108757.
[21] Ducreux É, Grouiez B, Robert S, Lepère M, Vispoel B, Gamache RR, et al. Measurements of H_2O broadened by CO_2 line-shape parameters: beyond the Voigt profile. J Quant Spectrosc Radiat Transf 2024;323:109026. https://doi.org/10.1016/j.jqsrt.2024.109026.
[22] Lavrentieva NN, Voronin BA, Fedorova AA. $H_2^{16}O$ line list for the study of atmospheres of Venus and Mars. Opt Spectrosc 2015;118:11–8. https://doi.org/10.1134/S0030400X15010178.
[23] Gamache RR, Farese M, Renaud CL. A spectral line list for water isotopologues in the 1100-4100 cm^{-1} region for application to CO_2-rich planetary atmospheres. J Mol Spectrosc 2016;326:144–50. https://doi.org/10.1016/j.jms.2015.09.001.
[24] Bézard B, de Bergh C, Crisp D, Maillard J-P. The deep atmosphere of Venus revealed by high-resolution nightside spectra. Nature 1990;345:508–11. https://doi.org/10.1038/345508a0.
[25] Bézard B, de Bergh C. Composition of the atmosphere of Venus below the clouds. J Geophys Res Planets 2007;112. https://doi.org/10.1029/2006JE002794.
[26] Bézard B, Fedorova A, Bertaux J-L, Rodin A, Korablev O. The 1.10- and 1.18-μm nightside windows of Venus observed by SPICAV-IR aboard Venus Express. Icarus 2011;216:173–83. https://doi.org/10.1016/j.icarus.2011.08.025.
[27] Fedorova A, Bézard B, Bertaux J-L, Korablev O, Wilson C. The CO_2 continuum absorption in the 1.10- and 1.18-μm windows on Venus from Maxwell Montes transits by SPICAV IR onboard Venus express. Planet Space Sci 2015:66–77. https://doi.org/10.1016/j.pss.2014.08.010. 113-114.
[28] Fedorova A, Marcq E, Luginin M, Korablev O, Bertaux J-L, Montmessin F. Variations of water vapor and cloud top altitude in the Venus' mesosphere from SPICAV/VEx observations. Icarus 2016;275:143–62. https://doi.org/10.1016/j.icarus.2016.04.010.
[29] Plateaux J-J, Regalia L, Boussin C, Barbe A. Multispectrum fitting technique for data recorded by Fourier transform spectrometer: application to N_2O and CH_3D. J Quant Spectrosc Radiat Transf 2001;68:507–20. https://doi.org/10.1016/S0022-4073(00)00040-6.
[30] Gordon IE, Rothman LS, Hargreaves RJ, Hashemi R, Karlovets EV, Skinner FM, et al. The HITRAN2020 molecular spectroscopic database. J Quant Spectrosc Radiat Transf 2022;277:107949. https://doi.org/10.1016/j.jqsrt.2021.107949.
[31] Loos J, Birk M, Wagner G. Measurement of positions, intensities and self-broadening line shape parameters of H_2O lines in the spectral ranges 1850-2280 cm^{-1} and 2390-4000 cm^{-1}. J Quant Spectrosc Radiat Transf 2017;203:119–32. https://doi.org/10.1016/j.jqsrt.2017.02.013.
[32] Conway EK, Gordon IE, Kyuberis AA, Polyansky OL, Tennyson J, Zobov NF. Calculated line lists for $H_2^{16}O$ and $H_2^{18}O$ with extensive comparisons to theoretical and experimental sources including the HITRAN2016 database. J Quant Spectrosc Radiat Transf 2020;241:106711. https://doi.org/10.1016/j.jqsrt.2019.106711.
[33] Gamache RR, Orphanos N, Vispoel B, Sung K, Toon GC. Measurements of H_2O-O_2 line shape parameters and the determination of the intermolecular potential for modified complex Robert-Bonamy calculations. Mol Phys 2023:e2281592. https://doi.org/10.1080/00268976.2023.2281592.
[34] Lyulin OM. Determination of spectral line parameters from several absorption spectra with the multispectrum fitting computer code. Atmos Ocean Opt 2015;28:487–95. https://doi.org/10.1134/S102485601506010X.
[35] Armstrong BH. Spectrum line profiles: the voigt function. J Quant Spectrosc Radiat Transf 1967;7:61–88. https://doi.org/10.1016/0022-4073(67)90057-X.
[36] Berman PR. Speed-dependent collisional width and shift parameters in spectral profiles. J Quant Spectrosc Radiat Transf 1972;12:1331–42. https://doi.org/10.1016/0022-4073(72)90189-6.
[37] Pickett HM. Effects of velocity averaging on the shapes of absorption lines. J Chem Phys 1980;73:6090–4. https://doi.org/10.1063/1.440145.
[38] Ngo NH, Tran H, Gamache RR, Hartmann JM. Pressure effects on water vapour lines: beyond the Voigt profile. Philos Trans R Soc Math Phys Eng Sci 2012;370:2495–508. https://doi.org/10.1098/rsta.2011.0272.
[39] Ngo NH, Lisak D, Tran H, Hartmann J-M. An isolated line-shape model to go beyond the Voigt profile in spectroscopic databases and radiative transfer codes. J Quant Spectrosc Radiat Transf 2013;129:89–100. https://doi.org/10.1016/j.jqsrt.2013.05.034.
[40] Robert D, Bonamy J. Short range force effects in semiclassical molecular line broadening calculations. J Phys 1979;40:923–43. https://doi.org/10.1051/jphys:019790040010092300.
[41] Ma Q, Tipping RH, Boulet C. Modification of the Robert-Bonamy formalism in calculating Lorentzian half-widths and shifts. J Quant Spectrosc Radiat Transf 2007;103:588–96. https://doi.org/10.1016/j.jqsrt.2006.08.001.
[42] Gamache RR, Lynch R, Neshyba SP. New developments in the theory of pressure-broadening and pressure-shifting of spectral lines of H2O: the complex Robert-Bonamy formalism. J Quant Spectrosc Radiat Transf 1998;59:319–35. https://doi.org/10.1016/S0022-4073(97)00123-4.
[43] Gamache RR, Lamouroux J, Laraia AL, Hartmann J-M, Boulet C. Semiclassical calculations of half-widths and line shifts for transitions in the 30012←00001 and 30013←00001 bands of CO_2, I: collisions with N_2. J Quant Spectrosc Radiat Transf 2012;113:976–90. https://doi.org/10.1016/j.jqsrt.2012.02.014.
[44] Gamache RR, Vispoel B, Renaud CL, Cleghorn K, Hartmann L. Vibrational dependence, temperature dependence, and prediction of line shape parameters for the H_2O-H_2 collision system. Icarus 2019;326:186–96. https://doi.org/10.1016/j.icarus.2019.02.011.
[45] Renaud CL, Cleghorn K, Hartmann L, Vispoel B, Gamache RR. Line shape parameters for the H_2O-H_2 collision system for application to exoplanet and planetary atmospheres. Icarus 2018;306:275–84. https://doi.org/10.1016/j.icarus.2017.10.016.
[46] Vispoel B, Cavalcanti JH, Gamache RR. Modified complex Robert-Bonamy calculations of line shape parameters and their temperature dependence for water vapor in collision with N_2. J Quant Spectrosc Radiat Transf 2019;228:79–89. https://doi.org/10.1016/j.jqsrt.2019.02.023.
[47] Vispoel B, Gamache RR. Modified Complex Robert-Bonamy calculations of line shape parameters for the CO_2-H_2O collision system. J Quant Spectrosc Radiat Transf 2024;316:108896. https://doi.org/10.1016/j.jqsrt.2024.108896.
[48] Shostak SL, Muenter JS. The dipole moment of water. II. Analysis of the vibrational dependence of the dipole moment in terms of a dipole moment function. J Chem Phys 1991;94:5883–90. https://doi.org/10.1063/1.460472.
[49] Flygare WH, Benson RC. The molecular Zeeman effect in diamagnetic molecules and the determination of molecular magnetic moments (g values), magnetic susceptibilities, and molecular quadrupole moments. Mol Phys 1971;20:225–50. https://doi.org/10.1080/00268977100100221.
[50] Luo Y, Ågren H, Vahtras O, Jorgensen P, Spirko V, Hettema H. Frequency-dependent polarizabilities and first hyperpolarizabilities of H_2O. J Chem Phys 1993;98:7159–64. https://doi.org/10.1063/1.464733.
[51] Haynes WM, Lide DR. CRC handbook of chemistry and physics. 92nd edition. CRC Press; 2011.
[52] Chetty N, Couling VW. Measurement of the electric quadrupole moments of CO_2 and OCS. Mol Phys 2011;109:655–66. https://doi.org/10.1080/00268976.2010.546375.
[53] Bogaard MP, Orr BJ, Buckingham AD. MPT international review of science, physical chemistry, series two. vol. 2 molecular structure and properties. London: Butterworths; 1975.
[54] Tanaka Y, Jursa AS, LeBlanc FJ. Higher ionization potentials of linear triatomic molecules. I. CO2. J Chem Phys 1960;32:1199–205. https://doi.org/10.1063/1.1730874.
[55] Rohart F, Mäder H. Nicolaisen H. Speed dependence of rotational relaxation induced by foreign gas collisions: studies on CH_3F by millimeter wave coherent transients. J Chem Phys 1994;101:6475–86. https://doi.org/10.1063/1.468342.
[56] Rohart F, Ellendt A, Kaghat F, Mäder H. Self and polar foreign gas line broadening and frequency shifting of CH3F: effect of the speed dependence observed by millimeter-wave coherent transients. J Mol Spectrosc 1997;185:222–33. https://doi.org/10.1006/jmsp.1997.7395.
[57] Tran H, Hartmann J-M. An isolated line-shape model based on the Keilson and Storer function for velocity changes. I. Theoretical approaches. J Chem Phys 2009;130:094301. https://doi.org/10.1063/1.3073758.
[58] Hartmann J-M, Boulet C, Robert D. Collisional effects on molecular spectra: laboratory experiments and models, consequences for applications. Elsevier; 2021.
[59] Lamouroux J, Gamache RR, Schwenke DW. Determination of the reduced matrix elements using accurate ab initio wavefunctions: formalism and its application to the vibrational ground state (000) of $H_2^{16}O$. J Quant Spectrosc Radiat Transf 2014;148:49–57. https://doi.org/10.1016/j.jqsrt.2014.06.011.
[60] Gamache RR, Vispoel B. On the temperature dependence of half-widths and line shifts for molecular transitions in the microwave and infrared regions. J Quant Spectrosc Radiat Transf 2018;217:440–52. https://doi.org/10.1016/j.jqsrt.2018.05.019.
[61] Gordon IE, Rothman LS, Gamache RR, Jacquemart D, Boone C, Bernath PF, et al. Current updates of the water-vapor line list in HITRAN: a new "Diet" for air-broadened half-widths. J Quant Spectrosc Radiat Transf 2007;108:389–402. https://doi.org/10.1016/j.jqsrt.2007.06.009.
[62] Devi VM, Benner DC, Sung K, Crawford TJ, Gamache RR, Renaud CL, et al. Line parameters for CO2- and self-broadening in the ν_1 band of $HD^{16}O$. J Quant Spectrosc Radiat Transf 2017;203:133–57. https://doi.org/10.1016/j.jqsrt.2017.01.032.
[63] Devi VM, Benner DC, Sung K, Crawford TJ, Gamache RR, Renaud CL, et al. Line parameters for CO2- and self-broadening in the ν_3 band of $HD^{16}O$. J Quant Spectrosc Radiat Transf 2017;203:158–74. https://doi.org/10.1016/j.jqsrt.2017.02.020.